Time Delay Control of Flyback CCM Inverter for PV Power Applications

Sooa Kim[1], Minsung Kim[1], Sungho Lee[2], and Jin S. Lee[1]

[1]Department of Creative IT Engineering, POSTECH, Pohang, Kyungbuk, Republic of Korea
[2]Department of Electrical Engineering, POSTECH, Pohang, Kyungbuk, Republic of Korea

***Abstract*—A flyback inverter in continuous conduction mode (CCM) operation has simple structure, high efficiency, and low cost. But, in CCM operation, the transfer function from the control input to the output current of the flyback inverter has right-half-plane zero, which causes slow and delayed response. To achieve fast response, Time-delay controller (TDC) is proposed, which consists of a linear controller and a time delay estimator. The time-delay estimator is one of the simplest and efficient estimator that can estimate the unknown dynamics and disturbance. The linear controller enables the closed loop system to achieve the desired dynamics. Numerical simulations are performed to validate the proposed control approach.**

***Index Terms*—Non-minimum phase system, module-integrated converter, utility disturbance, unknown dynamics.**

I. Introduction

In general photovoltaic (PV) power generation systems, the PV inverter system can be constructed in two ways: central inverter architecture and micro-inverter architecture [1]. In its early stage, central inverter architecture is used to connect 8 to 10 solar panels to the utility grid. This architecture is easy to implement and the cheapest option, so it is the preferred solution for large photovoltaic systems until now. But central inverter architecture is more sensitive to shading or cloudy weather; it may reduce the overall efficiency of the systems [2]. To solve the problem, micro-inverter architecture has been introduced. The micro-inverter can track the maximum power point of every solar panel, thereby achieving the maximum power point tracking (MPPT) efficiency very high and shading or clouding effects can be minimized [3].

The configuration of the micro-inverter can be classified as two-stage or single-stage. In its early stage, a two-stage scheme has been widely used [4]. It consists of a first stage that boosts the low dc voltage to higher dc voltage, and a second stage that converts the dc output voltage of the first stage to grid-compatible ac voltage. The two-stage scheme can be used for applications with wide input range because the first stage regulates the input voltage, but this scheme suffers from high cost and low efficiency [5]. As an alternative approach, a single-stage scheme has been suggested; it consists of one stage which converts the low dc output voltage of solar panel to grid-compatible ac voltage. This scheme uses fewer devices than the two-stage scheme does, and can expect low cost and high efficiency [6].

Numerous studies have been conducted on the single-stage micro-inverter. A flyback topology based micro-inverter is known to be more competitive than other topology based circuits because it is simple, cheap, high efficient, and comes with isolation property. The flyback inverters can operate in discontinuous conduction mode (DCM) or continuous conduction mode (CCM). Compared to flyback inverter in DCM operation, the flyback inverter operating in CCM enjoys lower current stress and higher efficiency. However, the CCM scheme is difficult to control because the transfer function from the control input to the output current has a right-half-plane zero (RHPZ), which depends on the system operating point. In flyback inverter under CCM operation, the controller should minimize the effects of RHPZ, because the widely varying RHPZ generates delay and degrades tracking speed [7]. Thus, the conventional controller cannot accurately control the flyback inverter in CCM.

To overcome the problem, a time-delay controller (TDC) is proposed for the flyback inverter that operates in CCM. The TDC consists of a time-delay estimator and linear controller. The time-delay estimator estimates unknown dynamics and disturbances and can be used to cancel them. The linear controller helps the closed loop system follow the desired dynamics. The TDC allows the flyback inverter in CCM to perform better than the previous flyback inverters do. To minimize the error that is produced by the time-delay estimation (TDE), the control system is designed to be operated in high switching frequency. Numerical simulations were performed to test the proposed TDC.

This paper is organized as follows. In Section II, the flyback inverter is modelled. In section III, a block diagram of the proposed controller is derived. The simulation results are shown in Section IV and experimental results are shown in Section V. Finally, the conclusion is drawn in Section VI.

II. Problem formulation

The input current is drawn from the PV panel to the flyback converter (Fig. 1). The H-bridge forms an unfold-

This research was supported by the MSIP(Ministry of Science, ICT and Future Planning), Korea, under the "IT Consilience Creative Program" (NIPA-2014-H0201-14-1001) supervised by the NIPA(National IT Industry Promotion Agency).

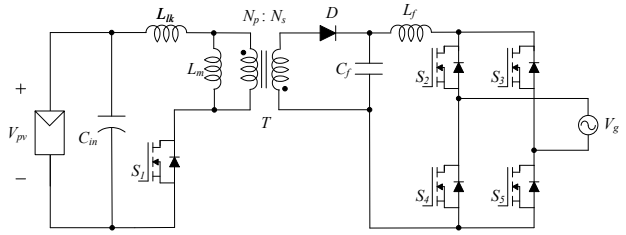

Fig. 1. The schematic diagram of the flyback converter.

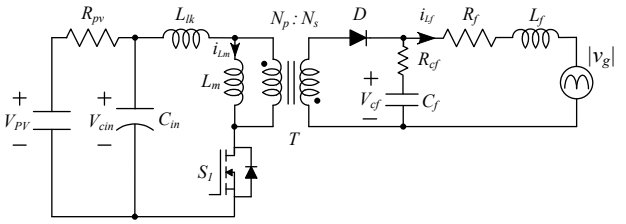

Fig. 2. The second-order model of the flyback converter.

ing circuit that unfolds the rectified sinusoidal current and supplys the resulting full sinusoidal ac current to the grid. An output filter reduces the harmonic components in the ac current.

The state-space equations that corresponds to the turn-on and turn-off periods can be expressed in the following equations, respectively,

$$\begin{aligned}\begin{bmatrix}\frac{dv_{C_{in}}(t)}{dt}\\ \frac{di_{L_m}(t)}{dt}\end{bmatrix} &= \begin{bmatrix}-\frac{1}{R_{pv}C_{in}} & -\frac{1}{C_{in}}\\ \frac{1}{L_m} & 0\end{bmatrix}\begin{bmatrix}v_{C_{in}}(t)\\ i_{L_m}(t)\end{bmatrix}\\ &\quad+\begin{bmatrix}\frac{1}{R_{pv}C_{in}} & 0\\ 0 & 0\end{bmatrix}\begin{bmatrix}V_{pv}(t)\\ v_g(t)\end{bmatrix},\\ \mathbf{y}(t) &= \begin{bmatrix}0 & 0\end{bmatrix}\begin{bmatrix}v_{C_{in}}(t)\\ i_{L_m}(t)\end{bmatrix},\end{aligned} \tag{1}$$

$$\begin{aligned}\begin{bmatrix}\frac{dv_{C_{in}}(t)}{dt}\\ \frac{di_{L_m}(t)}{dt}\end{bmatrix} &= \begin{bmatrix}-\frac{1}{R_{pv}C_{in}} & 0\\ 0 & 0\end{bmatrix}\begin{bmatrix}v_{C_{in}}(t)\\ i_{L_m}(t)\end{bmatrix}\\ &\quad+\begin{bmatrix}\frac{1}{R_{pv}C_{in}} & 0\\ 0 & -\frac{1}{nL_m}\end{bmatrix}\begin{bmatrix}V_{pv}(t)\\ v_g(t)\end{bmatrix},\\ \mathbf{y}(t) &= \begin{bmatrix}0 & \frac{1}{n}\end{bmatrix}\begin{bmatrix}v_{C_{in}}(t)\\ i_{L_m}(t)\end{bmatrix},\end{aligned} \tag{2}$$

where i_{L_m} is the current through the magnetizing inductor, $v_{C_{in}}$ is voltage across the capacitor, i_{L_f} is the current through the output inductor, v_{C_f} is the voltage across the output capacitor (Fig. 2).

Combining (1) and (2) using the state-space averaging method, the averaged model can be described as in [1]

$$\begin{aligned}\begin{bmatrix}\frac{dv_{C_{in}}(t)}{dt}\\ \frac{di_{L_m}(t)}{dt}\end{bmatrix} &= \begin{bmatrix}-\frac{1}{R_{pv}C_{in}} & -\frac{D_c(t)}{C_{in}}\\ \frac{D_c(t)}{L_m} & 0\end{bmatrix}\begin{bmatrix}v_{C_{in}}(t)\\ i_{L_m}(t)\end{bmatrix}\\ &\quad+\begin{bmatrix}\frac{1}{R_{pv}C_{in}} & 0\\ 0 & -\frac{1-D_c(t)}{nL_m}\end{bmatrix}\begin{bmatrix}V_{pv}(t)\\ v_g(t)\end{bmatrix},\\ \mathbf{y}(t) &= \begin{bmatrix}0 & \frac{1-D_c(t)}{n}\end{bmatrix}\begin{bmatrix}v_{C_{in}}(t)\\ i_{L_m}(t)\end{bmatrix},\end{aligned} \tag{3}$$

where $D_c(t)$ is the control duty.

Rearranging the right-hand side of (3), we have

$$\begin{aligned}\dot{\mathbf{x}}(t) &= \mathbf{A}\cdot\mathbf{x}(t)+\mathbf{B}(t)u_c(t)+\mathbf{E}\cdot\mathbf{v}(t), \qquad (4)\\ \mathbf{A} &= \begin{bmatrix}-\frac{1}{R_{pv}C_{in}} & 0\\ 0 & 0\end{bmatrix}, \mathbf{B}(t) = \begin{bmatrix}-\frac{i_{L_m}(t)}{C_{in}}\\ \frac{v_{C_{in}}(t)}{L_m}+\frac{v_g(t)}{nL_m}\end{bmatrix},\\ \mathbf{E} &= \begin{bmatrix}\frac{1}{R_{pv}C_{in}} & 0\\ 0 & -\frac{1}{nL_m}\end{bmatrix}\end{aligned}$$

where $\mathbf{x}(t) = [v_{C_{in}}(t), i_{L_m}(t)]^T$, $u_c(t) = D_c(t)$, and $\mathbf{v}(t) = [V_{pv}(t), v_g(t)]^T$ are the state vector, control input vector, and disturbance vector, respectively.

In steady-state under CCM, using the volt-second balance method to compute the magnetizing inductance L_m over one switching period T_s, we can obtain the nominal duty ratio $D_n(t)$ of the primary switch S_1:

$$D_n(t) = \frac{|v_g(t)|}{|v_g(t)|+nV_{pv}}. \tag{5}$$

The nominal duty ratio $D_n(t)$ performs to attenuate disturbances due to the grid voltage v_g and PV voltage V_{pv}. The control duty $D_c(t)$ then becomes $D_c(t) = D(t)+D_n(t)$ where $D(t)$ is TDC duty, which is the TDE output as shown in Fig. 3. Since the nominal duty has been applied to the dynamic system, (4) can be rewritten as

$$\dot{\mathbf{x}}(t) = \mathbf{A}\cdot\mathbf{x}(t)+\mathbf{B}(t)u(t)+\mathbf{E}\cdot\tilde{\mathbf{v}}(t), \tag{6}$$

where $u(t) = D(t)$ and $\tilde{\mathbf{v}}(t) = \mathbf{v}(t)-\hat{\mathbf{v}}(t)$, $\hat{\mathbf{v}}(t)$ is the estimated value of $\mathbf{v}(t)$.

Multiplying $\mathbf{B}^+(t)$ on the both side of equation (6), and rearranging the above equation, we have

$$u(t) = \mathbf{B}^+(t)\dot{\mathbf{x}}(t)+H(t). \tag{7}$$

where $\mathbf{B}^+(t) = (\mathbf{B}^T(t)\mathbf{B}(t))^{-1}\cdot\mathbf{B}^T(t)$, $H(t) = -\mathbf{B}^+(t)\mathbf{A}\cdot\mathbf{x}(t)-\mathbf{B}^+(t)\mathbf{E}\cdot\tilde{\mathbf{v}}(t)$.

III. Controller design

Let the desired trajectory be denoted by $\mathbf{x_r}(t)$. The control objective is to design a control law which $\mathbf{x}(t)$ is able to follow $\mathbf{x_r(t)}$. Defining $\mathbf{e}(t) = \mathbf{x_r}(t)-\mathbf{x}(t)$, we first select the target error dynamics as

$$\dot{\mathbf{e}}(t)+\mathbf{K_p}\mathbf{e}(t) = 0, \tag{8}$$

where $\mathbf{K_p} = diag(k_{p_1}, k_{p_2})$ is the proportional control gain that makes (8) become asymptotically stable.

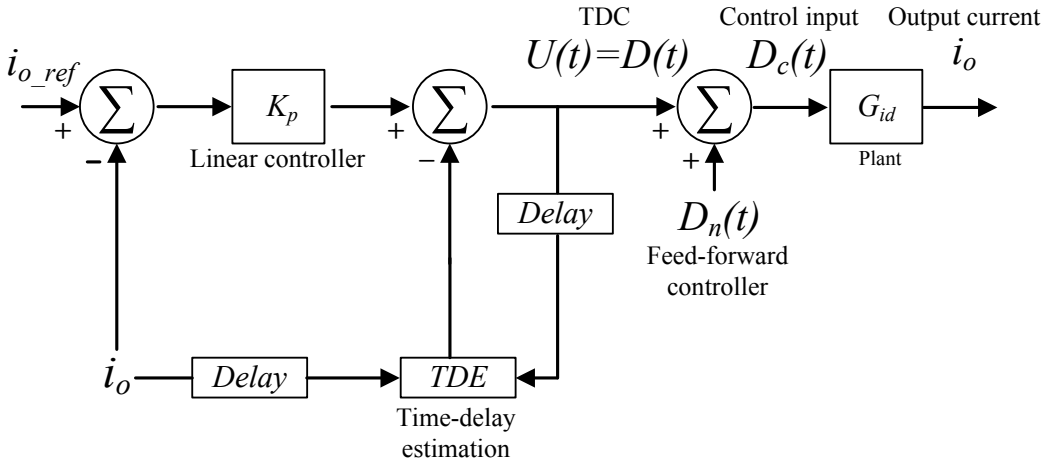

Fig. 3. The schematic diagram of the proposed controller. G_{id} is the control-input to output-current transfer function.

Let the control law be

$$u(t) = \mathbf{B}^{+}(t)(\dot{\mathbf{x}}_{\mathbf{r}}(t) + \mathbf{K_p}\mathbf{e}(t)) + \hat{H}(t), \tag{9}$$

where $\hat{H}(t)$ denotes the estimate of $H(t)$. If $\hat{H}(t)$ completely estimates $H(t)$, the target error dynamics (8) can be achieved, However, since the parameters in flyback converter dynamics are unknown and time-varying, it is not a trivial task to estimate $H(t)$. The time-delay estimation technique is one of the preferred techniques that can be adopted for this situation. From (7), $H(t)$ can be estimated as

$$\begin{aligned}\hat{H}(t) &= H(t-L) \\ &= u(t-L) - \mathbf{B}^{+}(t)\cdot\dot{\mathbf{x}}(t-L),\end{aligned} \tag{10}$$

where L is the time-delay (Fig. 4). It only needs time-delayed information of the state derivatives and the control input, and hence it is computationally simple and easy to implement. Substituting (10) to (9), we have the complete control input

$$\begin{aligned}u(t) = \mathbf{B}^{+}(t)(\dot{\mathbf{x}}_{\mathbf{r}}(t) + \mathbf{K_p}\mathbf{e}(t)) + u(t-L) \\ - \mathbf{B}^{+}(t)\cdot\dot{\mathbf{x}}(t-L).\end{aligned} \tag{11}$$

The overall control scheme is composed of three parts: the linear controller term that drives the closed-loop system to follow the target dynamics; the feed-forward term that attenuates the effect of disturbances on the system; the TDE term that eliminates the uncertain dynamics and remaining disturbances (Fig. 3). Remark 1. Even the CCM flyback PV inverter is bound to operate in both DCM and CCM operations; it inevitably operates in DCM at low instantaneous power level although it is designed to operate in CCM at rated power or above a certain power level. In the region of CCM, the input voltage is almost constant, and the output voltage varies in the small range. Then, we can simply use the constant input gain $\overline{\mathbf{B}}^{+}$ for easy implementation. As shown in Fig. 4, the waveform of magnetizing current in regions 1 and 2 are so similar that the time-delay estimation technique can be adopted. The resulting control input is described as

$$u(t) = \overline{\mathbf{B}}^{+}(\dot{\mathbf{x}}_{\mathbf{r}}(t) + \mathbf{K_p}\mathbf{e}(t)) + u(t-L) - \overline{\mathbf{B}}^{+}\cdot\dot{\mathbf{x}}(t-L). \tag{12}$$

IV. Simulation

To demonstrate feasibility of the developed controller, we conducted various computer simulations with a prototype model that is built using the parameters in Table I and simulated the proposed control scheme using PSIM software.

A conventional proportional controller cannot accurately control the flyback CCM inverter due to the existence of RHPZ. To solve the problem, a high gain controller can be used. However, as shown in Fig. 5, the system built with the high gain controller shows a large oscillation in CCM region when the controller gain increases from $\mathbf{K_p} = [0.05\ 0]^T$ to $\mathbf{K_p} = [0.08\ 0]^T$.

To overcome the limitation of the proportional con-

TABLE I
Parameters and components of the prototype.

Parameters	Symbols	Value
Voltage of solar panel	V_{pv}	60 V
Grid voltage	V_g	220 V_{rms}
Grid frequency	f	60 Hz
Transformer turns ratio	N_p:N_s	1:3.5
Magnetizing inductance	L_m	60 uH
Leakage inductance	L_{lk}	0.7 uH
Switching frequency	f_s	50 kHz
Input resistance	R_{pv}	0.1 ohm
Input capacitance	C_{in}	1000 uF
Filter inductance	L_f	0.5 mH
Filter capacitor resistance	R_f	0.1 ohm
Filter capacitance	C_f	0.68 uH
Filter inductor resistance	R_{cf}	0.1 ohm
Output power	P_O	250 W
Components	**Symbols**	**Part number**
MOSFET	S_1	IPP200N25N3G
Unfolding Switch	$S_2 - S_5$	IPP60R074C6
Transformer core	T	PQ3535
Diode	D	C2D05120A

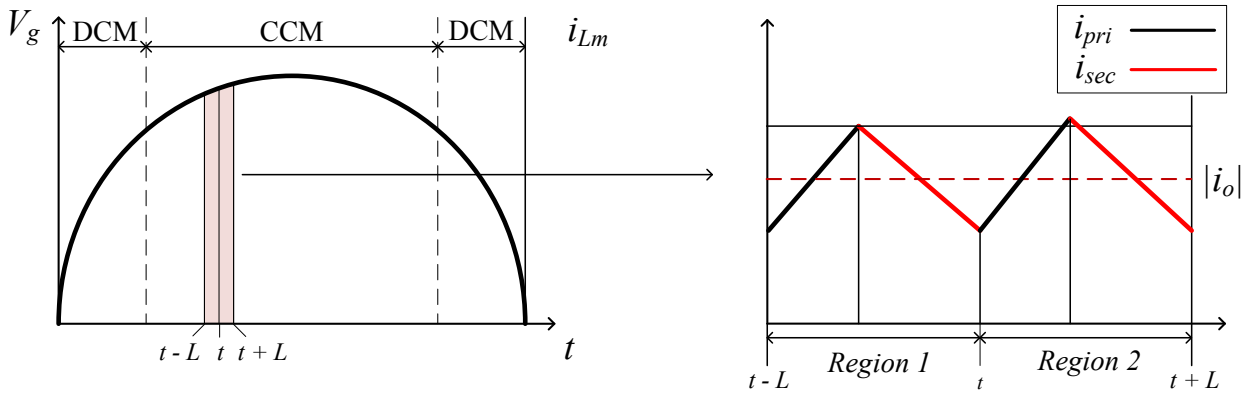

Fig. 4. The waveform of the magnetizing current in a single period in CCM.

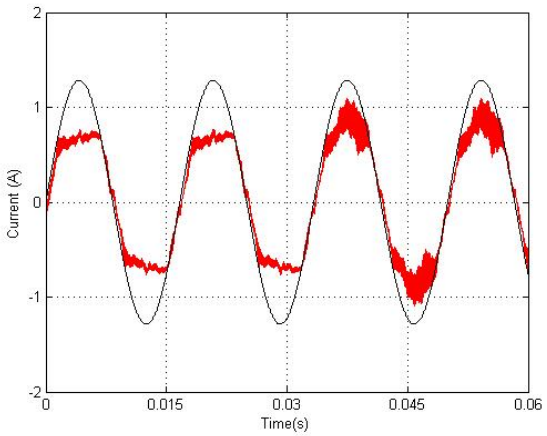

Fig. 5. Waveforms of the output current (red) and the desired output current (blue) when the proportional controller is used.

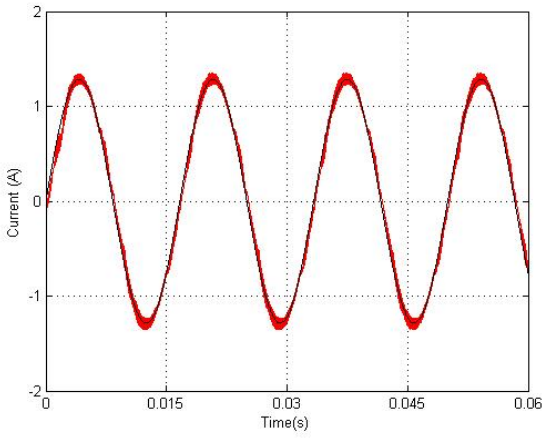

Fig. 6. Waveforms of the output current (red) and the desired output current (blue) when the proportional-integral controller is used.

troller, we can use a proportional-integral controller when the gains of proportional-integral controller are set to $\mathbf{K_p} = [0.05\ 0]^T$ and $\mathbf{K_i} = [85\ 0]^T$. An integral controller generates the control input to compensate the grid voltage disturbance so that the control performance can be improved. However, we can observe small oscillations at the peak current and at the DCM/CCM boundaries as in Fig. 6. They may severely increase the total harmonic distortion (THD) of the output current. To reduce these oscillations, we adopt the TDC can be adopted. As shown in Fig. 7, the proposed controller suppresses oscillations, and so the THD of the output current decreases. The TDE control input is shown in Fig. 8.

In the presence of the grid harmonics, the nominal

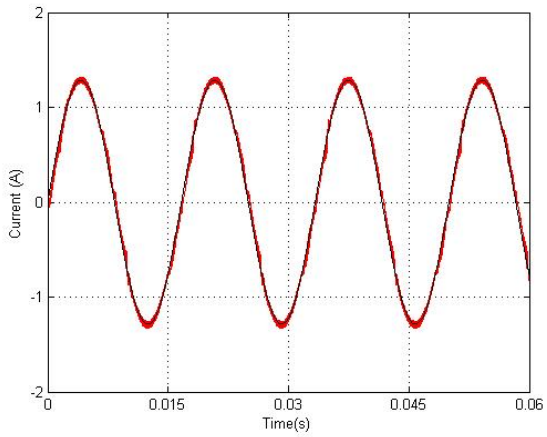

Fig. 7. Waveforms of the output current (red) and the desired output current (blue) when the proposed algorithm is applied.

duty cannot sufficiently attenuate the effect of grid voltage disturbance. Thus, when the conventional controller ($\mathbf{K_p} = [0.06\ 0]^T$, $\mathbf{K_p} = [85\ 0]^T$) is used, the output current cannot track the desired output current (Fig. 9), but, when the proposed controller is used, the output current tracks the desired output current better (Fig. 10). The TDE control input is shown in Fig. 11.

Fig. 12 shows the simulation results when the output power is unexpectedly changed from 200 W to 150 W. The power variation occurs at the peak current, and the output current immediately follows the reference current when the proposed controller is used. The TDE control input is shown in Fig. 13.

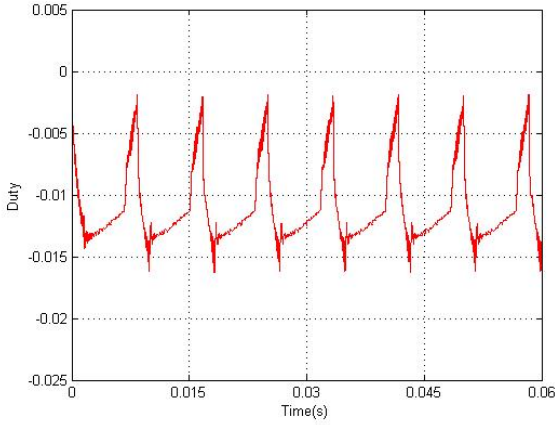

Fig. 8. Waveforms of the TDE control input.

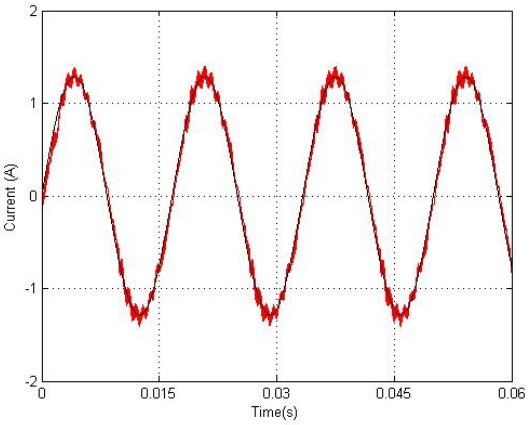

Fig. 9. Waveforms of the output current (red) and the desired output current (blue) when the feedforward and linear controllers are used.

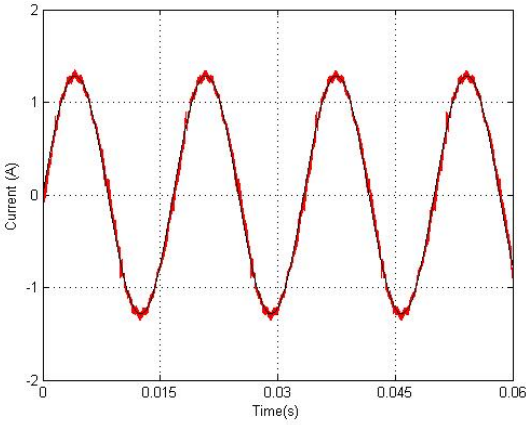

Fig. 10. Waveforms of the output current (red) and the desired output current (blue) when the proposed controller is used.

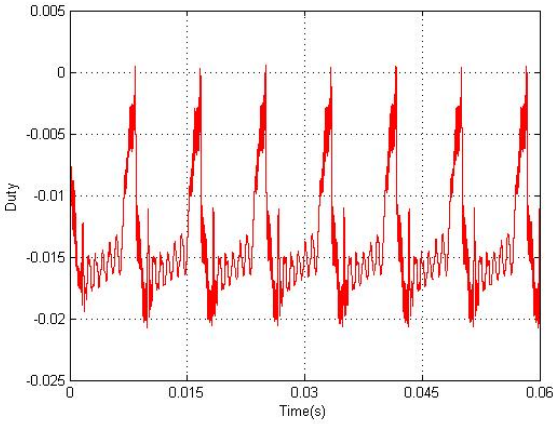

Fig. 11. Waveforms of the TDE control input.

V. Conclusion

This paper proposes a time-delay controller for flyback inverter in CCM operation. It is simple in structure, highly efficient, and cost effective. In contrast, the conventional controller shows poor control performance due to slow and delayed response in CCM operation. Feasibility of the time delay controller was demonstrated using the simulation results.

References

[1] F. F. Edwin, W. Xiao, and V. Khankikar, "Dynamic modeling and control of interleaved flyback module-integrated converter for PV power applications," *IEEE Trans. Ind. Electron.*, vol. 61, no. 3, pp. 1377-1388, Mar. 2014.

[2] S. B. Kjaer, J. K. Pedersen, and F. Blaabjerg, "A review of single-phase grid-connected inverters for photovoltaic modules," *IEEE Trans. Ind. Appl.*, vol. 41, no. 5, pp. 1292-1306, Sep./Oct. 2005.

[3] Y. H. Kim, J. W. Jang, S. C. Shin, and C. Y. Won, "Weighted-efficiency enhancement control for photo-voltaic AC module interleaved flyback inverter using a synchronous rectifier," *IEEE Trans. Power Electron.*, vol. 29, no. 12, pp. 6481-6493, Dec. 2014.

[4] G. Petrone, G. Spagnuolo, and M. Vitelli, "An analog technique for distributed MPPT PV applications," *IEEE Trans. Ind. Electron.*, vol. 59, no. 12, pp. 4713-4722, Dec. 2012.

[5] Li, Q., and Wolfs, P."A review of the single phase photo-voltaic module integrated converter topologies with three different DC link configurations," *IEEE Trans. Power Electron.*, *IEEE Trans. Power Electron.* 23(3), pp. 1320-1333, May 2008.

[6] Ji, Y. H., Jung, D. Y., Kim, J. H., Lee, T. W., and Won, C. Y., "A current shaping method for PV-AC module DCM-flyback inverter under CCM operation," *IEEE Trans. Power Electron.* and *ECCE Asia* (ICPE & ECCE), 2011 IEEE 8th International Conference on pp. 2598-2605, May 2011.

[7] F. Edwin, W. Xiao, and V. Khadkikar, "Topology review of single phase grid-connected module integrated convert-ers for PV applications," In IECON 2012-38th Annual Conference on *IEEE Ind. Electron. Society* pp. 821-827, Oct. 2012.

[8] D. K. Ryu, Y. H. Kim, J. G. Kim, C. Y. Won, and Y. C. Jung, "Interleaved active clamp flyback inverter using a synchronous rectifier for a photovoltaic AC module system," In Power Electronics and ECCE Asia (ICPE & ECCE), 2011 IEEE 8th International Conference on pp. 2631-2636. May 2011.

[9] Y. H. Kim, Y. H. Ji, J. G. Kim, Y. C. Jung, and C. Y. Won, "A new control strategy for improving weighted efficiency in photovoltaic AC module-type interleaved

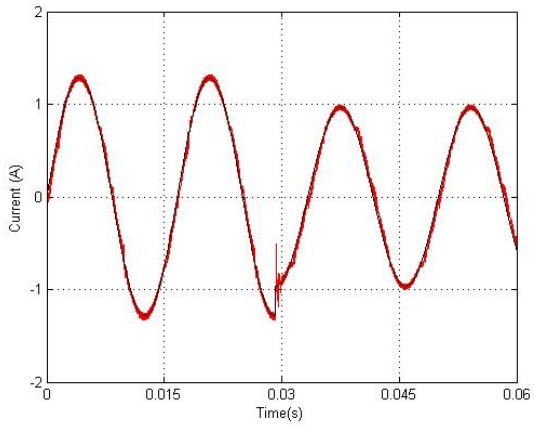

Fig. 12. Waveforms of the output current (red) and the desired output current (blue) when the output power is varied.

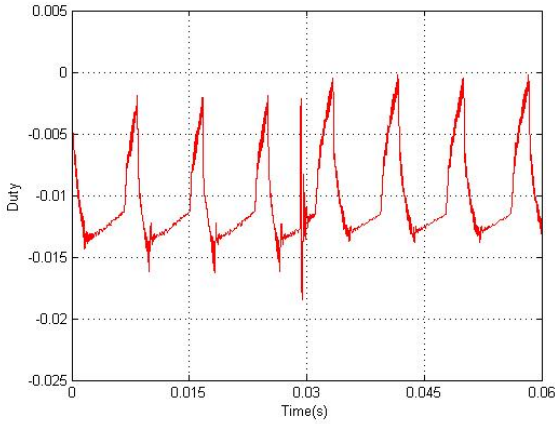

Fig. 13. Waveforms of the TDE control input.

flyback inverters," *IEEE Trans. Power Electron.*, 28(6), pp. 2688-2699, June 2013.

[10] Z. Zhang, X. F. He, and Y. F. Liu, "An optimal control method for photovoltaic grid-tied-interleaved flyback microinverters to achieve high efficiency in wide load range," *IEEE Trans. Power Electron.*, 28(11), pp. 5074-5087, Nov. 2013.

[11] M. Khalilian and E. Adib, "New Single-Stage Soft-Switching Photovoltaic Grid-Connected Flyback Micro-Inverter," In Electrical Power Distribution Conference (EPDC2014), May 2014.